Assessing the Effectiveness of SO_2, NOx, and NH_3 Emission Reductions in Mitigating Winter $PM_{2.5}$ in Taiwan Using CMAQ Model

Ping-Chieh Huang[1], Hui-Ming Hung[1*], Hsin-Chih Lai[2], and Charles C.-K. Chou[3]

[1]Department of Atmospheric Sciences, National Taiwan University, Taipei 106319, Taiwan
[2]Department of Green Energy and Environmental Resources, Chang Jung Christian University, Tainan 71101, Taiwan
[3]Research Center of Environmental Changes, Academia Sinica, Taipei 115201, Taiwan

Correspondence to: Hui-Ming Hung (hmhung@ntu.edu.tw)

Abstract. Taiwan experiences higher air pollution in winter when fine particulate matter ($PM_{2.5}$) levels frequently surpass national standards. This study employs the Community Multiscale Air Quality model to assess the effectiveness of reducing SO_2, NOx, and NH_3 emissions on $PM_{2.5}$ secondary inorganic species (i.e., SO_4^{2-}, NO_3^-, and NH_4^+). For sulfate, ~ 43.7% is derived from the chemical reactions of local SO_2 emission, emphasizing the substantial contribution of regional transported sulfate. In contrast, nitrate and ammonium are predominantly influenced by local NOx and NH_3 emissions. Reducing SO_2 emissions decreases sulfate levels, which in turn affects NH_3 partitioning and results in lower ammonium concentrations. Similarly, reducing NOx emissions lowers HNO_3, impacting nitrate and ammonium concentrations due to changes in HNO_3 and NH_3 partitioning. A particularly significant finding is that reducing NH_3 emissions decreases not only ammonium and nitrate but also sulfate by altering cloud droplet pH and SO_2 oxidation processes. While the impact of SO_2 reduction on $PM_{2.5}$ is less than NOx and NH_3, it emphasizes the complexity of regional sensitivities. Most of western Taiwan is NOx-sensitive, so reducing NOx emissions has a more substantial impact on lowering $PM_{2.5}$. However, given the higher mass emissions of NOx than NH_3 in Taiwan, NH_3 has a more significant consequence in mitigating $PM_{2.5}$ per unit mass emission reduction. The cost-effectiveness analysis suggests that NH_3 reduction outperforms SO_2 and NOx. Nevertheless, the costs of emission reduction vary due to differences in methodology and regional emission sources. Overall, this study considers both efficiency and costs, highlighting NH_3 emissions reduction as a promising strategy for $PM_{2.5}$ mitigation in the studied Taiwan's environment.

1 Introduction

Aerosol particles in the atmosphere have become a significant concern due to their adverse health effects (Maynard et al., 2002; Shiraiwa et al., 2017; Sugiyama et al., 2020) and their role in affecting global radiation budgets (Ramanathan et al., 2001; IPCC, 2021). Long-term exposure to air pollutants such as particulate matter (PM) and ozone (O_3) has been linked to millions of premature deaths annually on a global scale (Vohra et al., 2022; WHO, 2021). These findings emphasize the critical need for a comprehensive understanding of air pollution and effective management strategies to protect public health and mitigate environmental consequences.

PM can enter the atmosphere through direct emissions of primary aerosols, such as black carbon, sea salt, dust, and certain organic substances. Alternatively, PM can be formed via chemical reactions of gas-phase precursors, creating secondary aerosols such as sulfate (SO_4^{2-}), nitrate (NO_3^-), and ammonium (NH_4^+) (Seinfeld et al., 2006). The composition of PM varies globally, with organic and inorganic components representing major categories. Inorganic aerosol components, including sulfate, nitrate, ammonium, and chloride, constitute 35% to 77% of PM_1 worldwide (Schroder et al., 2018). The significant proportion of secondary inorganic composition can influence the pH value of PM, further impacting the formation of secondary organic matter (Zhang et al., 2007).

Sulfate is formed through both gas-phase and aqueous oxidation of sulfur dioxide (SO_2) emitted from sources like coal power plants and industrial processes, while nitrate is produced via the oxidation of nitrogen oxides (NOx), mainly emitted from traffic. Ammonium can be formed through the partitioning between the aqueous and gas phases of ammonia (NH_3) emitted from agricultural and industry sources. The overall sulfate-nitrate-ammonium formation processes are illustrated in Fig. 1. In addition to the gas phase reaction with OH radicals, SO_2 can also be oxidized by oxidants, such as hydrogen peroxide (H_2O_2) or ozone (O_3) in the aqueous phase. Due to the low volatility and high dissociation constant of sulfuric acid, most sulfuric acid is in the condensed phase and dissociates in aqueous particles. Ammonia and nitric acid are semi-volatile, so their dissolution in particles is determined by their Henry's law constant and dissociation constants. The presence of acid for ammonia or base for nitric acid can promote individual dissolution (Seinfeld et al., 2006). The interaction of sulfate, nitrate, and ammonium is vital in determining the quantity of PM.

Human activities and natural sources are responsible for releasing the inorganic aerosol precursors, i.e., SO_2, NOx, and NH_3. Reducing these emissions might mitigate $PM_{2.5}$ levels, thus improving air quality. Numerous studies have investigated emission reduction strategies, with a focus on NH_3 reductions showing promise in decreasing $PM_{2.5}$ levels (Chen et al., 2019; Gu et al., 2021). Liu et al. (2019) used the WRF-chem model to investigate emission reduction strategies in China and found that reducing SO_2 and NOx emissions alone does not significantly reduce total $PM_{2.5}$ levels. However, including controls for NH_3 emissions can reduce $PM_{2.5}$ by approximately 11-17%, but with the potential risk of exacerbating acid rain. Derwent et al. (2009) employed a photochemical trajectory model to simulate PM concentrations in the UK with 30% reductions in NH_3, SO_2, NOx, VOC, and CO emissions. In an ammonium-limited environment (southern UK), NH_3 emissions reductions had the most significant impact on PM reduction, exhibiting a non-linear dynamic effect.

In Taiwan, secondary inorganic aerosol constitutes 30-53% of $PM_{2.5}$, with sulfate, nitrate, and ammonium contributing significantly (16-32%, 2-24%, and 6-12%, respectively) (Chuang et al., 2021). $PM_{2.5}$ concentrations in Taiwan are usually higher in winter than in summer due to the meteorological conditions and the planetary boundary layer height. This effect is especially pronounced on the leeward side of the prevailing northeast monsoon in winter (i.e., western Taiwan), where $PM_{2.5}$ concentration accumulation is more significant (Hsieh et al., 2022; Hsu et al., 2016; Lai et al., 2020). Even though $PM_{2.5}$ concentration has decreased over the past two decades (Cheng et al., 2019; Chuang et al., 2021), the current $PM_{2.5}$ reduction effort might not efficiently meet the standard set by the Taiwan Ministry of Environment (TW-MOENV): a 24-hour standard of 35 μg m^{-3} and annual level of 15 μg m^{-3}. Given the complex interactions among secondary inorganic components and their substantial contribution to total PM in Taiwan, further research is imperative.

To study air pollution in Taiwan, we employed the Community Multiscale Air Quality (CMAQ) model, recognized for its comprehensiveness in simulating atmospheric chemical processes. The CMAQ model incorporates various chemical processes, including photolysis, multiphase chemistry, aerosol microphysics, aqueous chemistry in clouds, and cloud formation on particles (Byun et al., 2006). It is widely used to assess air pollutants on a regional scale and helps understand changes and mechanisms of pollutants under different scenarios. This study focuses on investigating the formation of secondary inorganic species, specifically sulfate, nitrate, and ammonium, during winter in Taiwan. By understanding the contribution of each composition contribution from different processes and their interaction, the reduction efficiency and cost of each aerosol precursor (i.e., SO_2, NOx, and NH_3) in mitigating $PM_{2.5}$ are evaluated.

2 Methodology

2.1 CMAQ model

The Community Multiscale Air Quality (CMAQ) model, using the Weather Research and Forecasting (WRF) model for meteorological conditions, was applied to simulate the concentrations of various chemical species over Taiwan. The WRF model version 3.7.1 (Skamarock et al., 2008) was initialized using a cold start and simulated the period from 28th November 2018 to 31st December 2018, with analysis focusing on December only. Four nested domains, as shown in Fig. S1a, were creased with horizontal resolutions of 81, 27, 9, and 3 km and a total of 45 vertical layers. The outer domain covers most of East Asia and the western Pacific, while the inner domain was dedicated to Taiwan.

The CMAQ model version 5.2.1 (Byun et al., 2006; Wyat Appel et al., 2018) was set up using the same horizontal grid structure as WRF, but with 15 vertical layers as seven layers under 1500 m and the top layer ~17 km above the ground. The inner domain of CMAQ consists of 135 × 90 grid cells. The chemical mechanism used in the simulations was Carbon Bond Mechanism version 6 and aerosol module version 6 with aqueous chemistry (cb6r3_ae6_aq). Emission data for Taiwan were from the Taiwan Emission Data System (TEDS9.0) based on the 2013 data. TEDS9.0 provides comprehensive information on various sources of pollutants in Taiwan, including industrial processes, transport, energy production, and residential

activities. Hourly model output data allowed for detailed temporal analysis. Additional details on the model configuration, including physical and chemical mechanisms, are summarized in Tables S1 and S2.

2.2 Observation data in Taiwan

The simulated data of the control run were compared with observations from ground-based monitoring stations to validate the model outputs. Hourly meteorological parameters (air temperature, relative humidity, and wind field) and pollutants (CO, O_3, and $PM_{2.5}$) data were collected from TW-MOENV air quality monitoring stations. Four stations along the western coast of Taiwan (Fig. S1b), including Tamsui (25.16° N, 121.45° E), Shalu (24.23° N, 120.57° E), Taixi (23.72° N, 102.20° E), and Qianzhen (22.61° N, 120.31° E) stations, were selected for comparisons of wind fields and $PM_{2.5}$ concentrations. Additionally, intensive observation data using filter sampling were obtained from Shalu (24.24° N, 120.57° E), Chung Shan Medical University (24.12° N, 120.65° E, CSMU), Zhushan (23.76° N, 120.68° E), and Xitou (23.67° N, 120.80° E) in central Taiwan from 1st December to 21st December 2018. These data provided further insights into $PM_{2.5}$ and its components. Sampling occurs from 9:00 to 18:00 for daytime samples and from 21:00 to 6:00 (next day) for nighttime samples. Inorganic ions were analyzed using ion chromatography (IC). More details on the analytical methodology can be found in Chen et al. (2021) and Lee et al. (2019).

2.3 CMAQ experimental design

To evaluate the contribution of the sulfate pathway and the impact of aerosol precursor emission reduction on mitigating $PM_{2.5}$ levels, we designed the following two series of experiments.

2.3.1 Sulfate sources

The local sulfate in $PM_{2.5}$ (PM-sulfate) can be contributed from transport and local gas phase and aqueous phase chemical reactions. To assess the contribution of each source to the local PM-sulfate within the inner domain, adjustments were made to the chemical reaction module within the CMAQ chemistry-transport model (CCTM). This analysis involved two simulations: "NoAqChem run" and "NoChem run". In NoAqChem run, sulfur aqueous phase oxidation reactions, including S(IV) oxidation by O_3, H_2O_2, organic peroxides, and metal ion catalysis (Jacobson, 1997), were turned off. In NoChem run, all chemical reactions in CMAQ were disabled. By comparing the PM-sulfate of these simulations with the control run, the contribution fractions of gas phase (F_{gas}) and aqueous phase (F_{aq}) reactions to local PM-sulfate were evaluated using the following equations:

$$F_{gas} = \frac{NoAqChem\ run - NoChem\ run}{Control\ run} \times 100\ \% \quad (1)$$

$$F_{aq} = \frac{Control\ run - NoAqChem\ run}{Control\ run} \times 100\% \ . \quad (2)$$

2.3.2 Emission reduction efficiency

Our study assessed variations in $PM_{2.5}$ and major inorganic composition concentrations resulting from emissions reductions. Specifically, we focused on modifying SO_2, NOx, and NH_3 emissions proportionally, as these are key aerosol precursors forming sulfate, nitrate, and ammonium in aerosols. The emissions of SO_2, NOx, and NH_3 are 1.18×10^6, 4.61×10^6, and 1.77×10^6 tons yr^{-1}, respectively, based on the applied emission inventory. Emissions were reduced individually at intervals of 0.2 (i.e., 0.8x, 0.6x, 0.4x, and 0.2x of the control-run emissions) in the inner domain, labeled as the "ER1 runs". Additionally, the effects of potential earlier emission quantities were explored by increasing emissions at 0.5 intervals (i.e., at 1.5x and 2.0x of the control-run emissions), referred to as "EI runs". Considering the interplay between nitrate and ammonium due to acid-base balance, we conducted "ER2 runs", reducing both NOx and NH_3 emissions at 0.2 intervals. Notably, "ER2 runs" covers the first half of December (from 1st to 14th December) to save computing resources, while other simulations encompassed the entire month. Table 1 provides a summary of all simulation settings.

The variation of aerosol composition and PM quantity based on emission adjustment is evaluated to assess the sensitivity and effectiveness of emission reduction. Following Takahama et al. (2004), a dimensionless sensitivity coefficient ($S_{X,Y}$) was introduced to evaluate the potential impacts of X emission reduction on Y (nitrate or $PM_{2.5}$) as follows:

$$S_{X,Y} = \frac{E_X}{Y}\frac{\mathrm{d}Y}{\mathrm{d}E_X} = \frac{\mathrm{dlog}(Y)}{\mathrm{dlog}(E_X)} \approx \frac{\Delta\log(Y)}{\Delta\log(E_X)}, \quad (3)$$

where E_X represents the specific emission of SO_2, NOx, and NH_3. $\Delta(var)$ is the difference between var_i and var_{i-1}, two adjacent points. For Y = nitrate, the sensitivity is sensitive to NOx or NH_3. A higher response among the given emission reductions indicated the properties of the environment, such as NOx-sensitive or NH_3-sensitive (Petetin et al., 2016). This framework can also assess the potential sensitivity of emission reductions on $PM_{2.5}$ concentration (i.e., $Y = PM_{2.5}$) for each emission. A higher sensitivity under E_X reduction indicates that more significant $PM_{2.5}$ mitigation can be achieved by controlling this emission.

2.4 Box model

A simplified box model, constructed using Python, was developed to study the influence of NH_3 emissions on sulfate formation, focusing specifically on the chemical reactions occurring in the aqueous phase. These reactions include dissolution, oxidation, and dissociation processes (Reactions 5-8 in Table 2). The model aimed to assess the impact of ammonia emission reduction on sulfate formation, considering only chemical processes with fixed meteorological conditions and no physical transport. The box model conditions were adapted from a grid point of CMAQ within the planetary boundary layer that exhibited sufficient liquid water content (LWC). To retrieve the initial concentrations of reactants, the maximum concentrations of oxidants (O_3 and H_2O_2) along the ammonia reduction profile were applied, with an equal amount of sulfate reverted to SO_2. The input parameters, including air temperature (T), liquid water content, and concentrations of SO_2, carbon dioxide (CO_2), total nitric acid (HNO_3), total NH_3, H_2O_2, O_3, S(IV), iron (Fe(III)), and manganese (Mn(II)), were from CMAQ and summarized in Table S3. Similar to the aqueous phase reactions in CMAQ, the dissolution of chemical components in

water follows the equilibrium between the gas and aqueous phases controlled by Henry's constants. The initial pH value was calculated based on the acid-base balance and charge balance of the system, ensuring consideration of different chemical species and their influence on the overall pH in the following equation:

$$[H^+] = [OH^-] + [HCO_3^-] + 2[CO_3^{2-}] + [HSO_3^-] + 2[SO_3^{2-}] + 2[SO_4^{2-}] + [NO_3^-] - [NH_4^+] \quad (4)$$

At each time step, the model calculated concentration changes based on the oxidation reactions, and the pH value was recalculated at the new equilibrium state. The oxidation reactions considered in the box model are as follows (Seinfeld et al., 2006):

$$SO_2 + O_3 + H_2O \rightarrow SO_4^{2-} + O_2 + 2H^+ \quad (R1)$$

$$HSO_3^- + O_3 \rightarrow SO_4^{2-} + O_2 + H^+ \quad (R2)$$

$$SO_3^{2-} + O_3 \rightarrow SO_4^{2-} + O_2 \quad (R3)$$

$$HSO_3^- + H_2O_2 + H^+ \rightarrow SO_4^{2-} + 2H^+ + H_2O \quad (R4)$$

$$S(IV) + \frac{1}{2}O_2 \xrightarrow{Mn^{2+},Fe^{3+}} S(VI), \quad (R5)$$

The rate constants for these reactions are summarized in Table S4.

Two sets of experiments were conducted to compare the results with those from CMAQ simulations. These experiments were conducted by gradually reducing NH_3 emissions in 0.1x intervals. The first set exclusively considered the oxidation reactions of S(IV) by O_3 and H_2O_2 (i.e., R2+R3), while the second set included additional oxidation reactions of S(IV) by O_2, catalyzed by iron and manganese (i.e., R2+R3+R4). The timestep of these experiments was set to 0.05 seconds, and results from a 10-minute run were analyzed. The oxidation reaction levels ranged from 65.1 to 99.9% of the 1-hour reaction, depending on the emission reduction ratio. The box model results reflect the impact of ammonia emission on sulfate formation under specific conditions. However, the composition of a grid box in CMAQ is influenced by chemical processes and transport, so the overall results between the box model and CMAQ may not match precisely.

2.5 Mitigation efficiency and cost estimation

To evaluate the effectiveness of $PM_{2.5}$ reduction, we employed an exponential function to fit $PM_{2.5}$ concentration as a function of emission adjustment ratios ranging from 0.2x to 2.0x of control-run emissions. The derivative of $PM_{2.5}$ concentration or the quantity of a specific component (Y) with respect to emissions was applied to assess the emission reduction efficiency of X (where X can be SO_2, NOx, or NH_3), denoted as follows:

$$Y\ reduction\ efficiency = \frac{dY}{dE_X}\ \ [\mu g\ m^{-3} \cdot ton^{-1} yr] \quad (5)$$

The cost of $PM_{2.5}$ reduction is evaluated by dividing the marginal abatement cost (MAC) by $PM_{2.5}$ reduction efficiency (obtained from Eq. (5) with Y as $PM_{2.5}$) as follows:

$$PM_{2.5}\ reduction\ cost = \frac{MAC}{PM_{2.5}\ reduction\ efficiency}\ \ [USD\ yr^{-1} \cdot \mu g^{-1} m^3]. \quad (6)$$

The applied MAC values are 421-1630 USD ton^{-1}, 8152-9570 USD ton^{-1}, and 1318-1400 USD ton^{-1} for SO_2, NOx, and NH_3, respectively, based on the studies of Gu et al. (2021) and Kaminski (2003).

3 Results and Discussion

3.1 Model performance

3.1.1 Meteorology

The comparison between WRF model results and TW-MOENV observations is presented in Tables 3 and S5, providing a comprehensive overview of monthly mean values, correlation coefficients (r), mean bias errors, mean absolute error, mean fractional bias, and mean fractional errors. Notably, the correlation coefficients for air temperature consistently exceed 0.8 across all four stations, showcasing a robust agreement. For relative humidity, the correlation coefficients range from 0.71 to 0.86, indicating a good alignment between observation and model results. For wind speed, the correlation coefficients range from 0.42 to 0.85 at these stations. The mean bias error at Shalu and Qianzhen meets the criteria suggested by Hu et al. (2016), while the mean absolute error at Tamsui, Shalu, and Qianzhen also meets the criteria. At Taixi, the model tends to be underestimated, resulting in a higher mean absolute error. Overall, these findings demonstrate satisfactory model performance. Wind fields play a critical role in the dispersion of air pollutants, affecting their transport and spatial distribution, not only for wind speed but for wind direction. Fig. S2 illustrates that the model reasonably captures the prevailing winter wind patterns, characterized by predominant winds blowing from the northeast. Although discrepancies in wind speed exist, with slight underestimations in Taixi and overestimations in Tamsui, Shalu, and Qianzhen, the overall trend of strong and weak winds is consistent between the model and observations.

3.1.2 Air pollutants

Table S5 also provides statistical results for pollutants. The correlation coefficients between observation and model range from 0.46 to 0.62 for CO and from 0.58 to 0.84 for O_3. The mean bias errors are higher for both CO and O_3, likely due to a significant underestimation of CO and an overestimation of O_3 in the model results. For $PM_{2.5}$, the model exhibits good agreement with observations, capturing similar concentration patterns. Specifically, lower $PM_{2.5}$ concentrations were observed under more vital northeasterly wind conditions, while weaker northeasterly winds or winds from other directions corresponded to higher pollutant concentrations. The correlation coefficients for $PM_{2.5}$ concentration range from 0.42 to 0.71, and the mean fractional bias and mean fractional error for $PM_{2.5}$ are within the acceptable criteria (Table 3), affirming the model's reliability (Fig. S2). For the spatial distribution of $PM_{2.5}$, high pollution levels are primarily concentrated in western regions, corresponding to densely populated areas (Fig. S3a). The $PM_{2.5}$ concentration gradually increases from north to south, mainly over flat land areas. To assess regional distribution, we used area average concentration and partitioning of $PM_{2.5}$, based on TW-MOENV's pollutant zone classification (Fig. S3b), focusing on areas with elevation less than 200 m above sea level (a.s.l.) to avoid

complexities in terrain. The partitioning of $PM_{2.5}$ is similar across regions, with secondary inorganic components constituting more than half of $PM_{2.5}$.

This study focuses on central Taiwan, specifically the marked red area on the map (Fig. S3b). In the control run, the surface layer mean $PM_{2.5}$ in central Taiwan shows a similar pattern to nitrate and ammonium, while sulfate has some slight differences (Fig. S4). The correlation coefficient between $PM_{2.5}$ and sulfate, nitrate, and ammonium are 0.65, 0.96, and 0.95, respectively. Given the high correlation between nitrate and ammonium ($r = 0.98$) and the significant contribution of nitrate to $PM_{2.5}$ concentrations in Taiwan, nitrate emerges as a major contributor to $PM_{2.5}$. Additionally, we observe that pollutant concentrations are related to the wind strength. Combined with Shalu's wind field time series, representing the environmental wind in central Taiwan, nitrate, ammonium, $PM_{2.5,}$ and wind speed show a certain negative correlation, while sulfate is less affected. This suggests that gaseous HNO_3 and NH_3 accumulate locally during weak wind conditions, facilitating the transformation of nitrate and ammonium into aerosol particles.

The correlation coefficients of $PM_{2.5}$ between observation and model at Shalu and CSMU are 0.76 and 0.65, respectively, demonstrating consistency of model results for concentration and change trend at these two stations (Fig. S5). However, the correlation between observation and model at Zhushan and Xitou is poor, likely due to the influence of the complex topography at these two places. Further analysis in Fig. S6 presents the trends and correlation coefficients for PM-sulfate, PM-nitrate, and PM-ammonium across the four stations. The data reveal a slight underestimation trend for PM-sulfate, particularly at Shalu and Zhushan. The simulation for PM-ammonium appears reasonably accurate, whereas PM-nitrate shows a tendency for overestimation. The simulated proportions of PM-sulfate, PM-nitrate, and PM-ammonium formation by CMAQ are 9.1-11.4%, 18.7-34.9%, and 9-13.7%, respectively. In contrast, the observation data indicates that proportions of PM-sulfate, PM-nitrate, and PM-ammonium formation are 13.9-19.6%, 16.6-22.8%, and 7.6-10.7%, respectively (Fig. 2). Considering the spatial heterogeneity of $PM_{2.5}$, our analysis focuses on examining the composition of $PM_{2.5}$ rather than emphasizing the differences between the model outputs and observational data. Overall, in central Taiwan's average model data and single-point observation data, secondary inorganic aerosols account for approximately half of the concentration of $PM_{2.5}$, with nitrate being the highest contributor.

3.2 Sulfate formation pathways

With the analysis of NoAqChem and NoChem runs, the mean contributions to sulfate in central Taiwan are as follows: 13.2% from gas reactions, 30.5% from aqueous reactions, and 56.3% from other processes. These other processes include transport from the domain boundary, locally emitted primary sulfate (constituting less than 5% of SO_2 emissions), and alterations of deposition. The analysis for other areas is summarized in Table S6, with all chemical processes accounting for less than 50% of the contributions. The major aqueous reactions occur in the cloud, typically with higher cloud water content (QC). Comparing the time series of average cloud water content in the boundary layer (Fig. S7a) shows that high QC corresponds to dominant aqueous chemical processes in sulfate formation. The correlation coefficient between QC and the sulfate difference

(control run - NoAqChem run) is 0.65, indicating the significant contribution of aqueous phase chemical processes. Additional correlation coefficients of PM composition and meteorological parameters are detailed in Table 4. Nitrate and ammonium concentrations exhibit a stronger relationship with the wind field, while sulfate concentration is more influenced by the occurrence of aqueous phase chemistry, specifically the amount of cloud water content in the atmosphere. In addition, the contribution of aqueous chemical processes is highly correlated with sulfate concentration in the control run, particularly during periods of elevated sulfate levels. However, these changes in sulfate have an insignificant impact on nitrate, ammonium, and $PM_{2.5}$ (Fig. S4). Given that nitrate constitutes a significant proportion of $PM_{2.5}$ during the winter in Taiwan, our results suggest that the overall trend of total $PM_{2.5}$ are more closely with the wind patterns (ventilation efficiency with nitrate formation) rather than solely the contributions from sulfate formed via aqueous phase chemistry.

3.3 Emission effects on surface layer $PM_{2.5}$

3.3.1 Trends in concentration

The impact of emission adjustments on $PM_{2.5}$ and its components in central Taiwan is shown in Fig. 3. $PM_{2.5}$ and secondary inorganic components show a decreasing trend as the emission ratio is reduced. When the emission ratio exceeds 1, the variation in $PM_{2.5}$ is relatively flat compared to when the emission ratio is below 1. This indicates a higher $PM_{2.5}$ mitigation efficiency for future emission reduction. Reductions in SO_2 primarily decrease sulfate and ammonium, while NOx reductions affect nitrate and ammonium. Conversely, NH_3 reductions decrease ammonium, nitrate, and sulfate levels. Since SO_2 is a precursor to sulfate, reducing SO_2 decreases sulfate formation, consequently modifying the ammonia partition and decreasing ammonium concentration (Tsimpidi et al., 2007). The negligible impact on nitrate can be attributed to nitric acid partition processes, which are affected by particle acidity and available aerosol water content. With decreased ammonium and sulfate, the available water content in aerosols decreases, adversely influencing nitric acid partitioning to aerosols. Although reduced sulfate formation promotes more nitric acid partitioning, thermodynamic calculations indicate that the reduced water content leads to a decline in dissolved nitrate.

For NOx, reducing NOx emissions results in a lower HNO_3 formation, leading to a significant reduction in PM-nitrate. The decreased acidity contribution from nitric acid alters the partition of ammonia, causing a decrease in ammonium. In contrast, the slight increase in sulfate formation may be attributed to enhanced chemical processes under lower NOx conditions. Reducing NOx emissions consumes less OH, a major pathway for HNO_3 formation during the daytime, as depicted in Reaction 2 of Table 2. The increased availability of OH can enhance the oxidation of SO_2 to form sulfuric acid through Reaction 1 in Table 2 (Derwent et al., 2009).

Regarding NH_3 emission reduction, NH_3 primarily acts as a base, influencing the dissolution of volatile acids such as HNO_3. Since nitrate has a higher molecular weight than ammonium, the most significant decrease in mass concentration is observed for nitrate. Sulfuric acid, with negligible volatility, predominantly remains in the aerosol phase. The observed decrease in

sulfate is likely due to altered chemical processes influenced by NH_3, particularly the aqueous reactions. The interplay between NH_3 reduction and sulfate formation will be discussed in more detail in Section 3.4.

With the significant $PM_{2.5}$ mitigation attributed to NOx or NH_3, the response of $PM_{2.5}$, sulfate, ammonium, and nitrate at various levels of NOx and NH_3 reduction are shown in Fig. S8. For a given reduction in NOx (or NH_3), the trends of interested species as a function of NH_3 (or NOx) are consistent with the case discussed in Fig. 3. When both emissions are reduced, the contour of $PM_{2.5}$ is concave upward, indicating that the mitigation efficiency is less than the linear combination of individual influence on $PM_{2.5}$. A similar pattern is observed for PM-nitrate and PM-ammonium, while PM-sulfate exhibits relatively smaller and different changes. These results suggest that changes in $PM_{2.5}$ concentration are mainly dominated by nitrate and ammonium, with sulfate having a minor effect on the studied environment. The deviation from the linear combination of individual contributions might be due to the variation in the partitioning between gas and aerosol phases under different acidity levels. For example, NH_3 might have an increased portion in the gas phase as NOx is decreased, while HNO_3 would have a higher portion in the gas phase as NH_3 is reduced. Further reduction of the other species would then reflect a higher portion reduction of gas phase concentration and a lower portion reduction of PM-related species. Therefore, it can be inferred that as emission reductions reach a certain level, the available nitric acid or ammonia is continuously reduced to low enough levels, potentially leading to a decline in the efficiency of $PM_{2.5}$ emission reduction (Veratti et al., 2023).

3.3.2 Sensitivity analysis

The sensitivity evaluation for different emission species on PM-nitrate and $PM_{2.5}$ is shown in Fig. 4. In the case of PM-nitrate sensitivity, S_{NOx,NO_3} increases as the emission ratio decreases and reaches a maximum value of 0.83 at an emission ratio around 0.4-0.8 (using control run as a base value). Subsequently, S_{NOx,NO_3} gradually decreases as the emission ratio continues to decrease. This transition is likely due to the available quantity of NO_2 for HNO_3 formation via the NO_2 + OH reaction. In addition to being produced by chemical reactions, HNO_3 concentration is also affected by the transported HNO_3 from the domain boundaries. While the transported HNO_3 concentration is relatively low compared to HNO_3 produced by local NOx emissions in Taiwan, its proportion gradually increases as NOx emissions decrease. When the HNO_3 concentration produced by the local chemical reaction is comparable to the transported concentration, the sensitivity coefficient decreases (detailed mathematical verification is provided in Section S1).

In contrast, S_{NH_3,NO_3} increases monotonically as the emission ratio decreases within the studied range, showing the significant influence of local NH_3 emission on PM-nitrate quantity. In the studied environmental context, a higher S_{NOx,NO_3} than S_{NH_3,NO_3} indicates that PM-nitrate is more sensitive to NOx emissions in central Taiwan. The sensitivity of PM-nitrate in spatial distribution (Fig. S9a) shows that the major cities in western Taiwan and the southwest offshore are in a NOx-sensitive environment, while only the eastern region is biased toward NH_3-sensitive, likely due to relatively low NH_3 and NOx emissions. As to the sensitivity on $PM_{2.5}$, the influence of NOx emissions reduction ($S_{NOx,PM_{2.5}}$) is similar to S_{NOx,NO_3}, as a reduction in NOx emissions primarily leads to a decrease in nitrate, exerting a dominant influence on $PM_{2.5}$ concentration. $S_{NH_3,PM_{2.5}}$ and

$S_{SO_2,PM_{2.5}}$ are relatively stable. $S_{SO_2,PM_{2.5}}$ gradually declines as the emission ratio decreases, while $S_{NH_3,PM_{2.5}}$ first increases as the emission ratio > 0.8 and then slightly decreases. For the overall emission ratio range studied, $S_{NH_3,PM_{2.5}}$ is around 0.19±0.01 while S_{NOx,NO_3} has a wider range from 0.05 to 0.24, and $S_{SO_2,PM_{2.5}}$ is 0.05±0.01. Under the studied condition (at the emission ratio of 0.9 in Fig. 4b), $S_{SO_2,PM_{2.5}}$ (~ 0.05) is the lowest, while $S_{NOx,PM_{2.5}}$ (~ 0.23) and $S_{NH_3,PM_{2.5}}$ (~ 0.2) are relatively higher, indicating that reducing NOx or NH_3 emissions results in a more significant reduction in $PM_{2.5}$ compared to reducing SO_2 emissions. The sensitivity on $PM_{2.5}$ in spatial distribution (Fig. S9b) and the statistical data for each area (Table S7) show that $S_{NOx,PM_{2.5}}$ is greater than $S_{NH_3,PM_{2.5}}$ in each air pollution zone, emphasizing the importance of NOx reduction in improving $PM_{2.5}$. However, in the northern, Chu-Miao, and central areas, $S_{NOx,PM_{2.5}}$ and $S_{NH_3,PM_{2.5}}$ are relatively similar. These areas have some white shading, indicating neutrality, and suggest that the reduction of NOx and NH_3 emissions is equally important.

3.4 Emission effects on sulfate formation

3.4.1 Composite results in cloud

The observed decrease in sulfate levels with a lower NH_3 emission ratio (Figs. 3c and S8b) is likely attributed to the modified cloud pH affecting aqueous phase sulfate production (Redington et al., 2009), as NH_3 emissions do not directly impact the gas-phase chemistry of SO_2. To capture the critical features, composite results from grid points containing clouds with significant SO_2 (i.e., a cloud water content ≥ 0.1 g kg^{-1} and SO_2 concentration ≥ 1 ppbv when NH_3 is at 0.2x) are depicted in Figs. S10 and S11 for land and sea regions, respectively. This categorization takes into account variations in pollutant levels between these two regions. The statistical summaries, including mean, 25th, and 75th percentile of cloud pH value and gaseous components, are provided in Table 4. While the mean pH values are higher over land than at sea, most grid points have a pH of 5, slightly below the average. Notably, grid points with lower pH values are predominantly characterized by NH_3 deficiency, especially at sea, where the concentrations of NH_3 are lower than on land.

The changes in chemical substances for both land and sea show consistent trends with emission reduction, featuring with higher concentrations of sulfate at sea compared to on land. The pattern of sulfate formation in clouds (Figs. S10b and S11b) is consistent with the average concentrations in the surface layer (Fig. S8b), increasing with NOx emission reduction and decreasing with NH_3 emission reduction. Conversely, the concentration change of SO_2 is opposite that of sulfate due to the conservation of sulfur. A decrease in sulfate concentration implies that more sulfur remains as SO_2 in the atmosphere, indicating weaker oxidation reactions. Furthermore, the reduction of NH_3 also impacts primary oxidants involved in sulfur oxidation, namely H_2O_2 and O_3. Intriguingly, the changes in H_2O_2 and O_3 exhibit opposite trends in response to NH_3 emission reduction (Figs. S10c and S10d), suggesting a potential influence on their oxidation rates. The aqueous oxidation pathways of SO_2 are strongly pH-dependent. The oxidation rate by H_2O_2 increases with pH < 3 and remains fairly constant at pH > 3 (Seinfeld et al., 2006). The other three reactions (O_3 and O_2 catalysis by Fe(III) and Mn(II)) are pH-dependent and increase with pH.

Overall, H_2O_2 oxidation is usually a major process. However, with an increase in pH, the oxidation rates of O_3 and O_2 catalysis via Fe(III) or Mn(II) might surpass that of H_2O_2 if high enough Fe(III) or Mn(II) relative to H_2O_2 presents.

3.4.2 Case analysis of a single grid point

The condition of a grid point along the coast of Taichung (24.203° N, 120.5053° E, the second layer ~ 68.5 m a.s.l.) at 8:00 am local time on 3rd December 2018 from CMAQ was selected for further analysis. This grid point fulfills our desired criteria, featuring a cloud water content of 0.376 g kg^{-1} and an SO_2 concentration of 7.13 ppbv. Figure 5 shows the concentrations of SO_2, H_2O_2, O_3, and acidity (i.e., $[H^+]$ in cloud water, calculated from CMAQ output data) at this grid point as a function of NH_3 and NOx emission ratios. With NH_3 emission reduction, SO_2 concentration increases significantly, especially when the NH_3 emission ratio falls below 0.4, while the concentration decreases slightly as NOx emission decreases. The pattern for acidity is similar to that of SO_2, showing an increase as NH_3 emissions decrease and a smooth decrease as NOx emissions decrease. This suggests a strong correlation between SO_2 and acidity, likely due to a common influencing factor, NH_3. As NOx emission decreases, the concentrations of both H_2O_2 and O_3 increase due to changes in gaseous chemical reactions that reduce the consumption of OH and O_3. When NH_3 emissions decrease, O_3 increases and H_2O_2 decreases. The trend might indicate that efficient SO_2 oxidation via the O_3 reaction dominates at a high NH_3 emission ratio. With O_3 in excess of SO_2, all SO_2 is completely reacted. As NH_3 emission is reduced to less than 0.6x, the increased acidity significantly slows SO_2 oxidation via the O_3 reaction, causing the system to switch to H_2O_2 oxidation. Therefore, the initial conditions for the box model can be derived using H_2O_2 concentration from the control run, the O_3 concentration from NH3_02x run, and SO_2 concentration as SO_2 in NH3_02x run, adjusted by adding H_2O_2 difference between the control run and the NH3_02x run to account for the consumed SO_2 by the H_2O_2 oxidation reaction. The initial value of SO_4 is calculated by subtracting the applied SO_2 initial concentration from the total S (PM-sulfate + SO_2 in the control run). A summary of the initial conditions is provided in Table S3.

Figure 6 shows the comparison between box model results and corresponding CMAQ results. Considering the main aqueous phase reactions involving O_3 and H_2O_2, the box model findings demonstrate that as the initial total NH_3 concentration decreases, the pH and H_2O_2 also decrease, while SO_2 and O_3 increase. These trends are consistent with the pattern observed in CMAQ but with some discrepancies. Specifically, in the box model, the concentration of SO_2 tends to be slightly higher at lower NH_3 emission ratios, whereas the concentrations of H_2O_2 and O_3 are lower than CMAQ results. Introducing additional oxidation reactions, i.e., the oxidation of tetravalent sulfur by O_2 with Fe(III) and Mn(II) catalysis in the system, brings the box model results closer to those of CMAQ. The box model demonstrates that higher NH_3 concentrations lead to higher pH values, resulting in O_3-dominated chemistry. The reduction of NH_3 emissions can increase environmental acidity, slow O_3 oxidation reactions, and gradually transition to an H_2O_2-dominated condition. However, in the studied environment, the concentration of H_2O_2 is lower than that of SO_2, resulting in residual SO_2 once H_2O_2 is depleted but causing a reduction in PM-sulfate.

3.5 Cost of emission reduction

The $PM_{2.5}$ reduction efficiency (Fig. 7a) based on the trend fitted in Fig. 3 increases as the emission ratio decreases across the three emission adjustment scenarios. Under the studied emission condition (i.e., emission ratio = 1), NH_3 reduction shows the highest efficiency, followed by SO_2, with NOx having the lowest. The increasing trend with the reduction ratio suggests a higher $PM_{2.5}$ reduction efficiency as the emission control policies continue. However, as discussed in Section 3.3, reducing SO_2 emissions has the least significant improvement in $PM_{2.5}$ levels. When the emission ratio is less than 0.8, the reduction efficiency of SO_2 emissions is exceeded by that of NOx emissions, indicating that the reduction capacity of SO_2 is the lowest. Additionally, the $PM_{2.5}$ reduction efficiency during relatively clean period and high pollution period is presented in Figs. S12a and S13a, respectively. During the clean period (6^{th} to 12^{th} December), NH_3 reduction maintains the highest efficiency, followed by SO_2 and NOx. However, during the high pollution period (16^{th} to 22^{nd} December), NH_3 reduction still has the highest efficiency, but NOx is higher than SO_2. This indicates that during high pollution periods, reducing SO_2 emission has a limited effect on the total amount of $PM_{2.5}$ concentration, and continued reducing SO_2 emission does not improve efficiency. The average results of these two different conditions explain the crossover pattern observed for SO_2 and NOx emission reduction in Fig. 7a.

Regarding policy considerations, cost becomes a crucial factor. Figs. 7b, S12b, and S13b illustrate the $PM_{2.5}$ reduction costs associated with these emission reduction experiments. We focus on the average results for December (Fig. 7b), the reduction of NOx emissions incurs the highest cost, amounting to approximately one billion dollars per year to achieve a 1 $\mu g\ m^{-3}$ reduction in $PM_{2.5}$ concentration. In comparison, the cost of SO_2 emission reduction ranges from tens of millions to 100 million dollars per year, while NH_3 emission reduction costs are around fifty million dollars per year. Therefore, performing NH_3 and SO_2 emission reductions would be more cost-efficient for achieving $PM_{2.5}$ reduction. However, cost evaluation involves uncertainties. Kaminski (2003) approach to estimating MAC of SO_2 focuses on power plants, discussing costs tied to emission control through alternative energy sources or equipment enhancements. On the other hand, Gu et al. (2021) employed the online Greenhouse Gas and Air Pollution Interactions and Synergies (GAINS) model to comprehensively assess the MAC of reducing NOx and NH_3 emissions across five continents and globally. Applying these methods to Taiwan may encounter uncertainties due to varying energy mixes, industrial structures, and environmental conditions in different regions. These distinctions could diverge from previous study assumptions, affecting the cost-effectiveness of emission reduction strategies. Additional factors, including meteorological patterns and technological landscapes, may introduce uncertainties in cost estimations. Furthermore, our study assumed a constant MAC value. In reality, MAC may vary as emissions decrease, usually becoming more expensive. Varied emission reduction approaches could result in substantial cost disparities, demanding careful consideration for regional applications. Therefore, a more comprehensive cost-benefit analysis, accounting for regional variations and potential changes in MAC with emission reduction, is crucial to devise effective and economically viable air pollution control strategies.

4 Conclusion

This study investigates the impacts of emission reduction on $PM_{2.5}$ and the secondary inorganic components (sulfate, nitrate, and ammonium) while assessing the effectiveness of emission reduction strategies in central Taiwan using the CMAQ model for December 2018. In our simulations, the mean $PM_{2.5}$ concentration in central Taiwan was 21.1 μg m^{-3}, comprising 2.7 μg m^{-3} of sulfate, 6.3 μg m^{-3} of nitrate, 2.6 μg m^{-3} of ammonium and other species including organics. For sulfate, 43.7% comes from chemical processes, with 30.5% from aqueous reactions and 13.2% from gas-phase reactions.

In evaluating emission reduction strategies, it was observed that reducing SO_2 emission has a less significant impact on mitigating $PM_{2.5}$ compared to reductions in NOx and NH_3 emissions. This is attributed to the fact that SO_2 emission reduction primarily affects sulfate, which constitutes only 12% of $PM_{2.5}$ in this study. On the other hand, reductions of NOx or NH_3 emission led to substantial decreases in nitrate and ammonium, effectively mitigating $PM_{2.5}$. However, a non-linear effect was noted between the reductions of NOx and NH_3 emissions, indicating that the mitigating effects of these two emissions are not linearly additive. Through sensitivity analysis, the impact of NOx or NH_3 emission reduction on $PM_{2.5}$ is relatively similar in northern Taiwan, Chu-Miao area, and central Taiwan, while the Yun-Chia-Nan area and Kao-Ping area show a preference for NOx emission reduction. Notably, NH_3 emission reduction affects sulfur chemical reactions in the aqueous phase through changing pH values in cloud droplets, shifting the primary oxidant from ozone to H_2O_2, which is a limited agent in this study. The sensitivity of the S(IV) to S(VI) oxidation reaction to acidity was verified using a box model. The oxidations by O_2 catalyzed via Fe(III) and Mn(II) were also found to significantly contribute to the sulfur oxidation, as demonstrated by the box model. Other research has highlighted the importance of metal ion-catalyzed sulfur oxidation reactions in sulfate formation, with this pathway contributing up to 19% of sulfate formation in China during winter (Huang et al., 2014).

Emission reduction strategies to combat $PM_{2.5}$ are crucial but entail considerable costs. Our comprehensive analysis shows that, considering both efficiency and cost, reducing NH_3 emissions is the most effective strategy for the studied Taiwan's environmental conditions. However, it is imperative to acknowledge that NH_3 emissions are mainly associated with industrial, agricultural, and livestock activities. Industrial ammonia manufacturing has historically boosted global food production and population (Erisman et al., 2008), and green ammonia may also play a significant role in future carbon-free energy endeavors (Chehade et al., 2021; Kang et al., 2015). Therefore, exploring large-scale emission reduction strategies and carefully assessing potential issues, such as aerosol pH changes leading to increased acid rain (Liu et al., 2019), are vital areas for further research. Overall, this study provides valuable insights into the intricate interactions among air pollutants and their impacts on $PM_{2.5}$, highlighting the ongoing need for continued efforts to reduce emissions and improve air quality in Taiwan.

Code availability

The code is not publicly accessible, but readers can contact HM Hung (hmhung@ntu.edu.tw) for more information.

Data availability

The CMAQ model output and TW-MOENV observation data used in this study can be accessed online at https://doi.org/10.5281/zenodo.10623526.

Author contributions

PC Huang set up experiments, ran experiments, and prepared the draft. HM Hung supervised the project, including data discussion and manuscript editing. HC Lai provided the control run of WRF and CMAQ model. CCK Chou provided IC analysis of $PM_{2.5}$.

Competing interests

The authors declare that they have no conflict of interest.

Acknowledgments

This study is supported by National Science and Technology Council (NSTC), Taiwan under grants of 111-2111-M-002-009 and 112-2111-M-002-014. We acknowledge the valuable insights from Dr. Ruijun Dang at Harvard and Prof. Jen-Ping Chen at National Taiwan University for the sensitivity analysis discussion.

References

Byun, D., and Schere, K. L.: Review of the Governing Equations, Computational Algorithms, and Other Components of the Models-3 Community Multiscale Air Quality (CMAQ) Modeling System, Appl. Mech. Rev., 59, 51-77, 10.1115/1.2128636, 2006.

Chehade, G., and Dincer, I.: Progress in green ammonia production as potential carbon-free fuel, Fuel, 299, 120845, https://doi.org/10.1016/j.fuel.2021.120845, 2021.

Chen, C.-L., Chen, T.-Y., Hung, H.-M., Tsai, P.-W., Chou, C. C. K., and Chen, W.-N.: The influence of upslope fog on hygroscopicity and chemical composition of aerosols at a forest site in Taiwan, Atmos. Environ., 246, 118150, https://doi.org/10.1016/j.atmosenv.2020.118150, 2021.

Chen, Y., Shen, H., and Russell, A. G.: Current and Future Responses of Aerosol pH and Composition in the U.S. to Declining SO_2 Emissions and Increasing NH_3 Emissions, Environ. Sci. Technol., 53, 9646-9655, 10.1021/acs.est.9b02005, 2019.

Cheng, F.-Y., and Hsu, C.-H.: Long-term variations in $PM_{2.5}$ concentrations under changing meteorological conditions in Taiwan, Sci. Rep., 9, 6635, 10.1038/s41598-019-43104-x, 2019.

Chuang, M.-T., Chou, C. C. K., Hsiao, T.-C., Lin, K.-y., Lin, N.-H., Lin, W.-Y., Wang, S.-H., Pani, S. K., and Lee, C.-T.: Analyzing the increasing importance of nitrate in Taiwan from long-term trend of measurements, Atmos. Environ., 267, 118749, https://doi.org/10.1016/j.atmosenv.2021.118749, 2021.

Derwent, R., Witham, C., Redington, A., Jenkin, M., Stedman, J., Yardley, R., and Hayman, G.: Particulate matter at a rural location in southern England during 2006: Model sensitivities to precursor emissions, Atmos. Environ., 43, 689-696, https://doi.org/10.1016/j.atmosenv.2008.09.077, 2009.

Erisman, J. W., Sutton, M. A., Galloway, J., Klimont, Z., and Winiwarter, W.: How a century of ammonia synthesis changed the world, Nature Geoscience, 1, 636-639, 10.1038/ngeo325, 2008.

Gu, B., Zhang, L., Van Dingenen, R., Vieno, M., Van Grinsven, H. J. M., Zhang, X., Zhang, S., Chen, Y., Wang, S., Ren, C., Rao, S., Holland, M., Winiwarter, W., Chen, D., Xu, J., and Sutton, M. A.: Abating ammonia is more cost-effective than nitrogen oxides for mitigating $PM_{2.5}$ air pollution, Science, 374, 758-762, 10.1126/science.abf8623, 2021.

Hsieh, M.-K., Chen, Y.-W., Chen, Y.-C., and Wu, C.-M.: The Roles of Local Circulation and Boundary Layer Development in Tracer Transport over Complex Topography in Central Taiwan, Journal of the Meteorological Society of Japan. Ser. II, 100, 555-573, 10.2151/jmsj.2022-028, 2022.

Hsu, C.-H., and Cheng, F.-Y.: Classification of weather patterns to study the influence of meteorological characteristics on $PM_{2.5}$ concentrations in Yunlin County, Taiwan, Atmos. Environ., 144, 397-408, https://doi.org/10.1016/j.atmosenv.2016.09.001, 2016.

Hu, J., Chen, J., Ying, Q., and Zhang, H.: One-year simulation of ozone and particulate matter in China using WRF/CMAQ modeling system, Atmos. Chem. Phys., 16, 10333-10350, 10.5194/acp-16-10333-2016, 2016.

Huang, X., Song, Y., Zhao, C., Li, M., Zhu, T., Zhang, Q., and Zhang, X.: Pathways of sulfate enhancement by natural and anthropogenic mineral aerosols in China, J. Geophys. Res. Atmos., 119, 14,165-114,179, https://doi.org/10.1002/2014JD022301, 2014.

IPCC: Climate Change 2021: The Physical Science Basis. Contribution of Working Group I to the Sixth Assessment Report of the Intergovernmental Panel on Climate Change, edited by: Masson-Delmotte, V., Zhai, P., Pirani, A., Connors, S. L., Péan, C., Berger, S., Caud, N., Chen, Y., Goldfarb, L., Gomis, M. I., Huang, M., Leitzell, K., Lonnoy, E., Matthews, J. B. R., Maycock, T. K., Waterfield, T., Yelekçi, O., Yu, R., and Zhou, B., Cambridge University Press, Cambridge, United Kingdom and New York, NY, USA, 2021.

Jacobson, M. Z.: Development and application of a new air pollution modeling system—II. Aerosol module structure and design, Atmos. Environ., 31, 131-144, https://doi.org/10.1016/1352-2310(96)00202-6, 1997.

Kaminski, J.: Technologies and costs of SO_2-emissions reduction for the energy sector, Appl. Energy, 75, 165-172, https://doi.org/10.1016/S0306-2619(03)00029-1, 2003.

Kang, D. W., and Holbrook, J. H.: Use of NH_3 fuel to achieve deep greenhouse gas reductions from US transportation, Energy Reports, 1, 164-168, https://doi.org/10.1016/j.egyr.2015.08.001, 2015.

Lai, H.-C., and Lin, M.-C.: Characteristics of the upstream flow patterns during PM2.5 pollution events over a complex island topography, Atmos. Environ., 227, 117418, https://doi.org/10.1016/j.atmosenv.2020.117418, 2020.

Lee, C. S. L., Chou, C. C. K., Cheung, H. C., Tsai, C. Y., Huang, W. R., Huang, S. H., Chen, M. J., Liao, H. T., Wu, C. F., Tsao, T. M., Tsai, M. J., and Su, T. C.: Seasonal variation of chemical characteristics of fine particulate matter at a high-elevation subtropical forest in East Asia, Environ. Pollut., 246, 668-677, https://doi.org/10.1016/j.envpol.2018.11.033, 2019.

Liu, M., Huang, X., Song, Y., Tang, J., Cao, J., Zhang, X., Zhang, Q., Wang, S., Xu, T., Kang, L., Cai, X., Zhang, H., Yang, F., Wang, H., Yu, J. Z., Lau, A. K. H., He, L., Huang, X., Duan, L., Ding, A., Xue, L., Gao, J., Liu, B., and Zhu, T.: Ammonia emission control in China would mitigate haze pollution and nitrogen deposition, but worsen acid rain, Proc. Natl. Acad. Sci. U.S.A., 116, 7760-7765, doi:10.1073/pnas.1814880116, 2019.

Maynard, A. D., and Maynard, R. L.: A derived association between ambient aerosol surface area and excess mortality using historic time series data, Atmos. Environ., 36, 5561-5567, https://doi.org/10.1016/S1352-2310(02)00743-4, 2002.

Petetin, H., Sciare, J., Bressi, M., Gros, V., Rosso, A., Sanchez, O., Sarda-Estève, R., Petit, J. E., and Beekmann, M.: Assessing the ammonium nitrate formation regime in the Paris megacity and its representation in the CHIMERE model, Atmos. Chem. Phys., 16, 10419-10440, 10.5194/acp-16-10419-2016, 2016.

Ramanathan, V., Crutzen, P. J., Kiehl, J. T., and Rosenfeld, D.: Aerosols, Climate, and the Hydrological Cycle, Science, 294, 2119-2124, 10.1126/science.1064034, 2001.

Redington, A. L., Derwent, R. G., Witham, C. S., and Manning, A. J.: Sensitivity of modelled sulphate and nitrate aerosol to cloud, pH and ammonia emissions, Atmos. Environ., 43, 3227-3234, https://doi.org/10.1016/j.atmosenv.2009.03.041, 2009.

Schroder, J., Campuzano-Jost, P., Day, D., Shah, V., Sullivan, A., Campos, T., Reeves, J., Hills, A., Guo, H., Fibiger, D., McDuffie, E., Weber, R., Apel, E., Jaeglé, L., Brown, S., Thornton, J., and Jimenez, J.: Sources and Secondary Production of Organic Aerosols in the Northeastern United States during WINTER, J. Geophys. Res. Atmos., 123, 10.1029/2018JD028475, 2018.

Seinfeld, J. H., and Pandis, S. N.: Atmospheric Chemistry and Physics: From Air Pollution to Climate Change, Wiley, 2006.

Shiraiwa, M., Ueda, K., Pozzer, A., Lammel, G., Kampf, C. J., Fushimi, A., Enami, S., Arangio, A. M., Fröhlich-Nowoisky, J., Fujitani, Y., Furuyama, A., Lakey, P. S. J., Lelieveld, J., Lucas, K., Morino, Y., Pöschl, U., Takahama, S., Takami, A., Tong, H., Weber, B., Yoshino, A., and Sato, K.: Aerosol Health Effects from Molecular to Global Scales, Environ. Sci. Technol., 51, 13545-13567, 10.1021/acs.est.7b04417, 2017.

Skamarock, W. C., Klemp, J. B., Dudhia, J., Gill, D. O., Barker, D. M., Duda, M. G., Huang, X., Wang, W., and Powers, J. G.: A Description of the Advanced Research WRF Version 3, U.S. National Center for Atmospheric Research, Boulder, Colorado, NCAR/TN–475+STR, 2008.

Sugiyama, T., Ueda, K., Seposo, X. T., Nakashima, A., Kinoshita, M., Matsumoto, H., Ikemori, F., Honda, A., Takano, H., Michikawa, T., and Nitta, H.: Health effects of $PM_{2.5}$ sources on children's allergic and respiratory symptoms in Fukuoka, Japan, Sci. Total Environ., 709, 136023, https://doi.org/10.1016/j.scitotenv.2019.136023, 2020.

Takahama, S., Wittig, A. E., Vayenas, D. V., Davidson, C. I., and Pandis, S. N.: Modeling the diurnal variation of nitrate during the Pittsburgh Air Quality Study, J. Geophys. Res. Atmos., 109, D16S06, 10.1029/2003JD004149, 2004.

Tsimpidi, A. P., Karydis, V. A., and Pandis, S. N.: Response of Inorganic Fine Particulate Matter to Emission Changes of Sulfur Dioxide and Ammonia: The Eastern United States as a Case Study, J. Air Waste Manage. Assoc., 57, 1489-1498, 10.3155/1047-3289.57.12.1489, 2007.

Veratti, G., Stortini, M., Amorati, R., Bressan, L., Giovannini, G., Bande, S., Bissardella, F., Ghigo, S., Angelino, E., Colombo, L., Fossati, G., Malvestiti, G., Marongiu, A., Dalla Fontana, A., Intini, B., and Pillon, S.: Impact of NOx and NH_3 Emission Reduction on Particulate Matter across Po Valley: A LIFE-IP-PREPAIR Study, Atmosphere, 14, 10.3390/atmos14050762, 2023.

Vohra, K., Marais, E. A., Bloss, W. J., Schwartz, J., Mickley, L. J., Van Damme, M., Clarisse, L., and Coheur, P.-F.: Rapid rise in premature mortality due to anthropogenic air pollution in fast-growing tropical cities from 2005 to 2018, Science Advances, 8, eabm4435, 10.1126/sciadv.abm4435, 2022.

WHO: Review of evidence on health aspects of air pollution: REVIHAAP project: technical report, World Health Organization. Regional Office for Europe, Copenhagen, 2021.

Wyat Appel, K., Napelenok, S., Hogrefe, C., Pouliot, G., Foley, K. M., Roselle, S. J., Pleim, J. E., Bash, J., Pye, H. O. T., Heath, N., Murphy, B., and Mathur, R.: Overview and Evaluation of the Community Multiscale Air Quality (CMAQ) Modeling System Version 5.2, Air Pollution Modeling and its Application XXV, Cham, 2018.

Zhang, Q., Jimenez, J. L., Worsnop, D. R., and Canagaratna, M.: A Case Study of Urban Particle Acidity and Its Influence on Secondary Organic Aerosol, Environ. Sci. Technol., 41, 3213-3219, 10.1021/es061812j, 2007.

Tables

Table 1: Experimental design.

Experiments	Descriptions
Control run	Use mechanism cb6r3ae6aq
NoAqChem run	Turn off sulfur aqueous phase oxidation reactions
NoChem run	Turn off all chemistry reactions
ER1 runs	SO_2, NOx, and NH_3 emissions reduced by ratios of 0.8, 0.6, 0.4, and 0.2 separately
ER2 runs	Both NOx, and NH_3 emissions reduced by ratios of 0.8, 0.6, 0.4, and 0.2 (only 12/1~12/14)
EI runs	SO_2, NOx, and NH_3 emissions increased by ratios of 1.5 and 2.0 separately

Table 2: The applied chemical reactions related to the formation of sulfate, nitrate, and ammonium.

		Reaction
Gas phase	1.	$SO_{2(g)} + OH_{(g)} \rightarrow HSO_{3(g)} \rightarrow\rightarrow H_2SO_{4(g)}$
	2.	$NO_{2(g)} + OH_{(g)} \rightarrow HNO_{3(g)}$
	3.	$N_2O_{5(g)} + H_2O \rightarrow 2HNO_{3(g)}$
Aqueous phase	4.	$H_2SO_{4(aq)} \rightarrow SO_{4(aq)}^{2-} + 2H^+$
	5.	$S(IV)_{(aq)} + Oxidants_{(aq)} \rightarrow SO_4^{2-} + 2H^+$ * S(IV): H_2SO_3, HSO_3^-, SO_3^{2-} * Oxidants: O_3, H_2O_2, MHP, PAA, O_2
	6.	$NH_{3(g)} \leftrightarrow NH_{3(aq)} \leftrightarrow NH_{4(aq)}^+ + OH^-$
	7.	$HNO_{3(g)} \leftrightarrow HNO_{3(aq)} \leftrightarrow NO_{3(aq)}^- + H^+$
	8.	$H^+ + OH^- \rightarrow H_2O$

Table 3: Statistic of wind and $PM_{2.5}$ of MOENV observation and model simulation for four stations.

	Tamsui	Shalu	Taixi	Qianzhen	[a]Criteria
Wind speed (m/s)					
Mean value of MOENV	1.99	4.52	7.52	2.07	
Mean value of WRF	3.25	4.73	4.85	2.33	
Correlation coefficient	0.46	0.85	0.69	0.42	
Mean bias error	1.22	0.21	-2.70	0.25	$\leq \pm 0.5$
Mean absolute error	1.56	1.11	3.00	0.77	≤ 2.0
$PM_{2.5}$ concentration (μg m^{-3})					
Mean value of MOENV	10.75	16.09	20.93	31.72	
Mean value of CMAQ	12.12	19.70	15.97	40.56	
Correlation coefficient	0.59	0.70	0.71	0.42	
Mean bias error	1.42	3.72	-4.79	8.88	
Mean absolute error	8.02	9.36	10.37	15.02	
Mean fractional bias	-0.32	0.21	-0.48	0.19	$\leq \pm 0.6$
Mean fractional error	0.71	0.56	0.66	0.40	≤ 0.75

[a]The crieteria are suggested by Hu et al. (2016).

$$\text{Correlation coefficient} = \frac{\sum_{i=1}^{n}(m_i-\bar{m})(o_i-\bar{o})}{\sqrt{\sum_{i=1}^{n}(m_i-\bar{m})^2}\sqrt{\sum_{i=1}^{n}(o_i-\bar{o})^2}}$$

$$\text{Mean bias error} = \overline{(m_i - o_i)}$$

$$\text{Mean absolute error} = \overline{|(m_i - o_i)|}$$

$$\text{Mean fractional bias} = 2 \times \overline{\left(\frac{m_i-o_i}{m_i+o_i}\right)}$$

$$\text{Mean fractional error} = 2 \times \overline{\left|\left(\frac{m_i-o_i}{m_i+o_i}\right)\right|}$$

where m_i and o_i are the wind speed or concentrations of model and observation at time i, respectively, and $\bar{m}$ and $\bar{o}$ are the average values over December 2018.

Table 4: Correlation coefficients of $PM_{2.5}$, sulfate, nitrate, ammonium, and meteorological parameters (WS and QC) of control run for central Taiwan.

	$PM_{2.5}$	SO_4^{2-}	NO_3^-	NH_4^+	dSO_4^{2-}
SO_4^{2-}	0.65	-	-	-	0.73
NO_3^-	0.97	0.61	-	-	-
NH_4^+	0.95	0.77	0.98	-	-
WS	-0.54	-0.34	-0.51	-0.52	-
QC	0.05	0.43	0.07	0.18	0.65

WS is the single-point wind speed of the surface layer in Shalu.
QC is the average cloud water within the planetary boundary layer in central Taiwan.
dSO_4^{2-} is the sulfate difference concentration (control run – NoAqChem run).

Table 5: Statistics of pH in cloud droplets and the concentration of gaseous components in both land (32130 grid points) and sea (122316 grid points) regions.

	Land			Sea		
Variables	**Mean**	**Q1**	**Q3**	**Mean**	**Q1**	**Q3**
pH	5.15	5.00	5.00	5.01	5.00	5.00
SO_2 (ppbv)	1.65	1.01	1.96	1.68	1.16	1.90
NH_3 (ppbv)	2.10	0.03	0.84	0.42	0.02	0.16
HNO_3 (ppbv)	0.37	0.11	0.51	1.42	0.61	1.72
H_2O_2 (ppbv)	0.06	0.003	0.06	0.05	0.002	0.03
O_3 (ppbv)	44.6	38.9	51.3	48.2	43.2	53.6

Mean: Arithmetic mean; Q1: 25th percentile; Q3: 75th percentile.

565 **Figures**

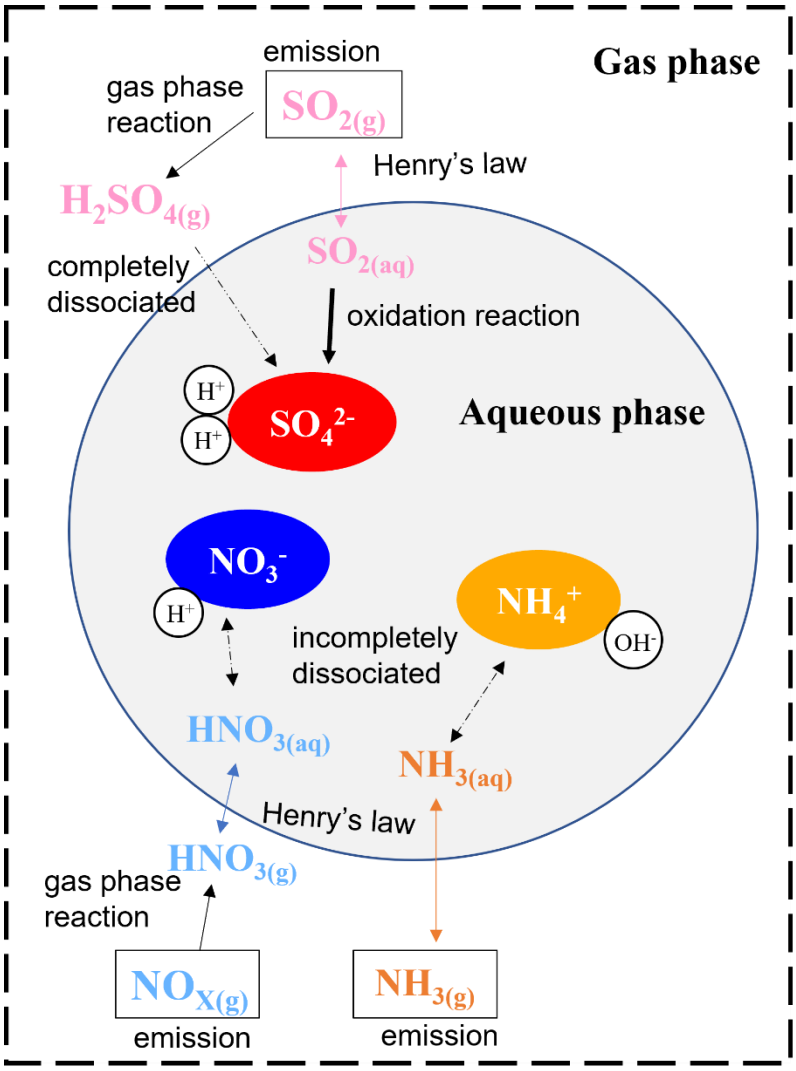

Figure 1: Schematic diagram of chemical interactions in sulfate-nitrate-ammonium formation.

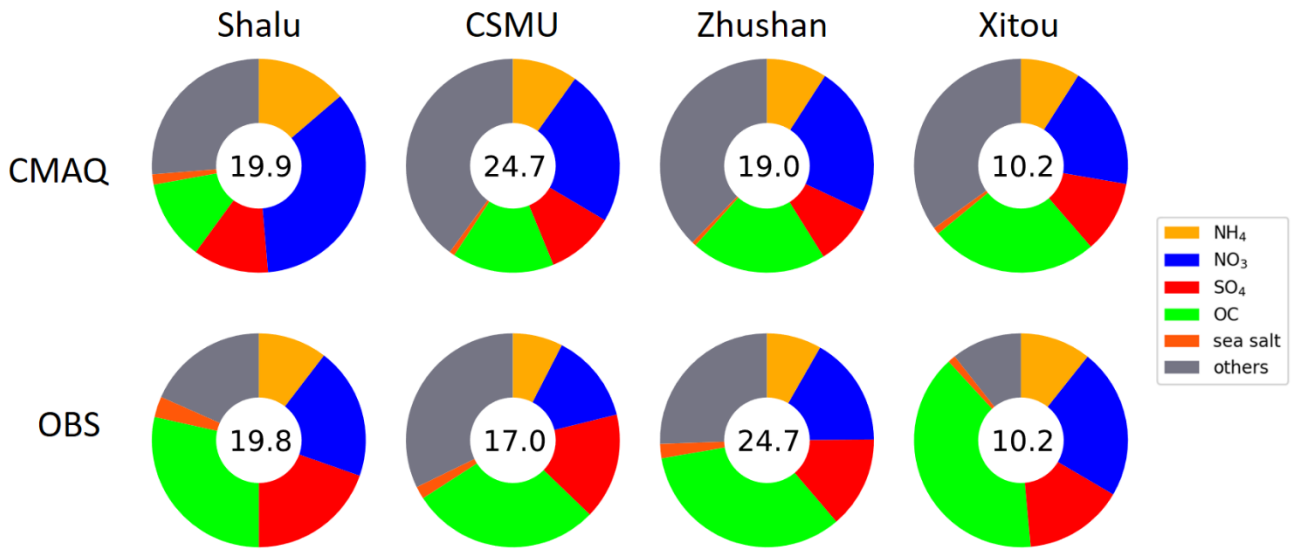

Figure 2: Comparison of $PM_{2.5}$ components between intensive observation data and CMAQ surface layer data for four sites ($PM_{2.5}$ concentration indicated inside the circle in μg m^{-3}). Individual components are shown in the legend, with colors arranged in a clockwise direction from the top. Conditions: mean values from 1st to 21st December 2018 for each station (OBS) or grid point (CMAQ).

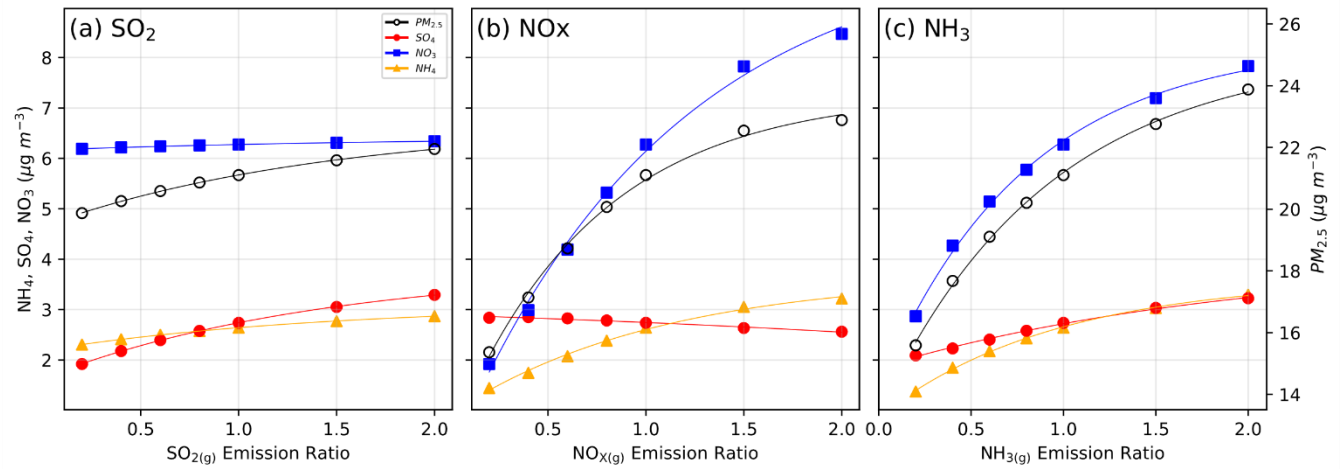

Figure 3: The response of $PM_{2.5}$ and major secondary inorganic components (sulfate, nitrate, and ammonium) to the emission ratio of (a) SO_2, (b) NOx, and (c) NH_3. Lines are the fitting results using an exponential function. Conditions: average data for December 2018 at the surface layer of central Taiwan.

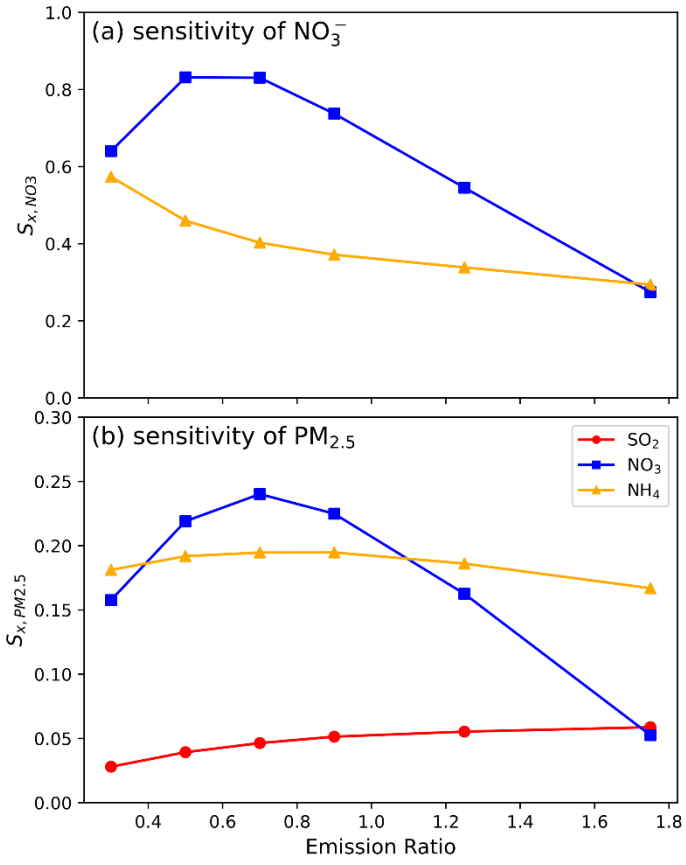

Figure 4: (a) Nitrate sensitivity as a function of emission ratio for NOx (S_{NOx,NO_3}) and NH_3 (S_{NH_3,NO_3}) and (b) $PM_{2.5}$ sensitivity as a function of emission ratio for SO_2 ($S_{SO_2,PM_{2.5}}$), NOx ($S_{NOx,PM_{2.5}}$) and NH_3 ($S_{NH_3,PM_{2.5}}$) . Data are calculated using the first-order difference, with the x-axis representing the mean values of the two points involved in the differencing process. Conditions: average data for December 2018 at the surface layer of central Taiwan.

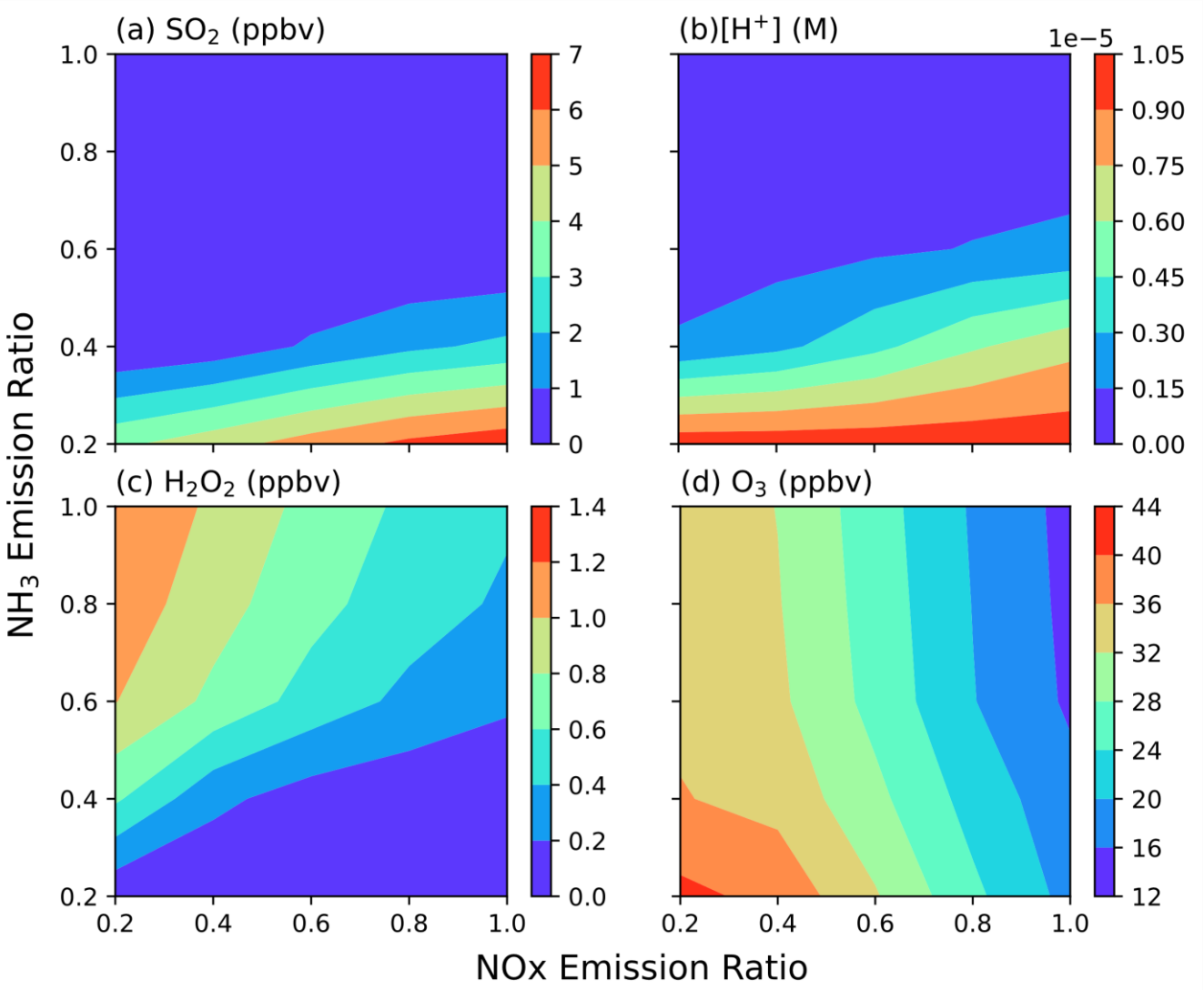

Figure 5: (a) SO_2, (b) H^+, (c) H_2O_2, and (d) O_3 concentrations as a function of NOx (x-axis) and NH_3 (y-axis) emission ratios for a single grid point. Conditions: data for 08:00 am LT on 3rd December 2018, at an altitude of 68.5 m a.s.l. for the location of (24.2° N, 120.5° E).

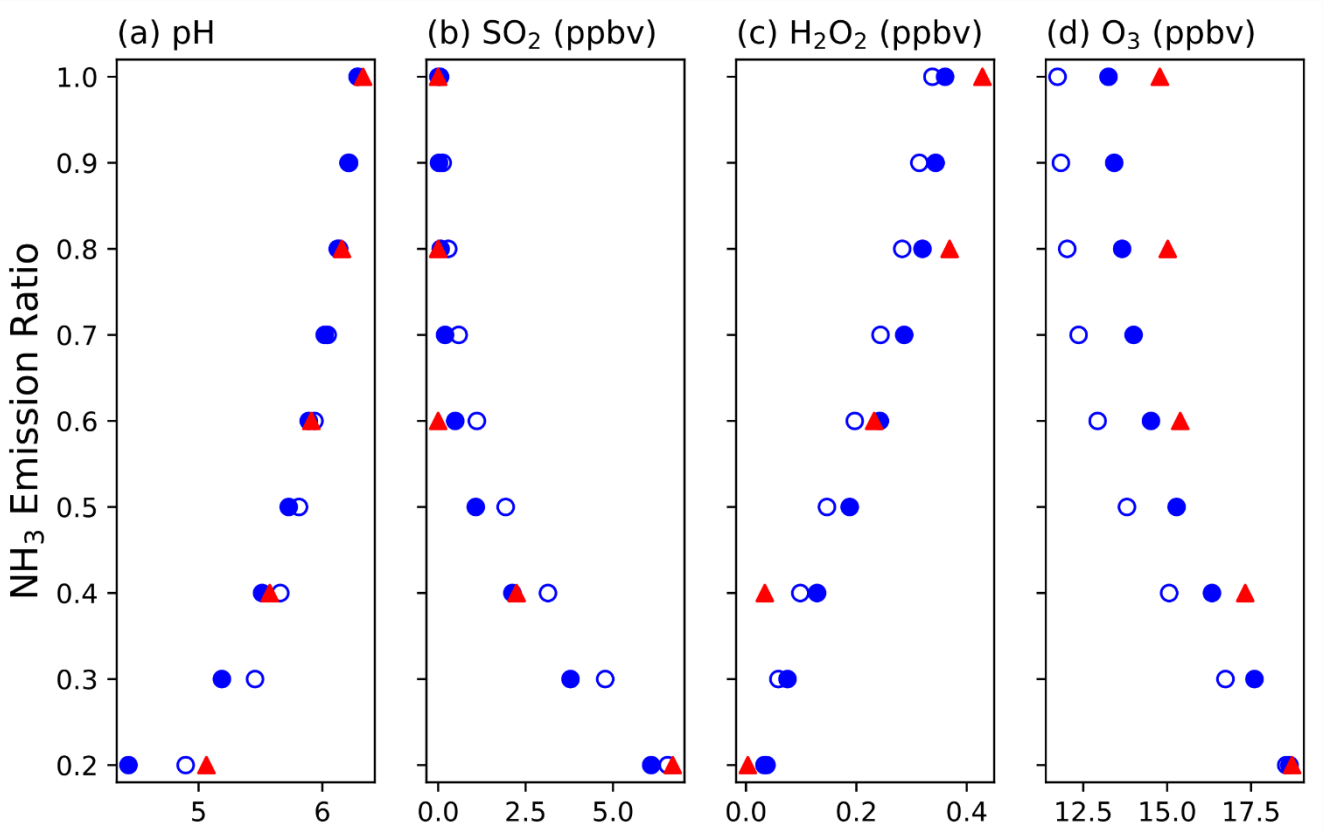

Figure 6: The comparison between CMAQ and box model results for (a) pH and the concentrations of (b) SO_2, (c) H_2O_2, and (d) O_3as a function of NH_3 emission ratio. Red triangle points: CMAQ model results; blue open circles: box model with H_2O_2 and O_3 reactions; blue solid circles: box model with H_2O_2, O_3, and O_2 catalyzed by Fe(III) and Mn(II) reactions.

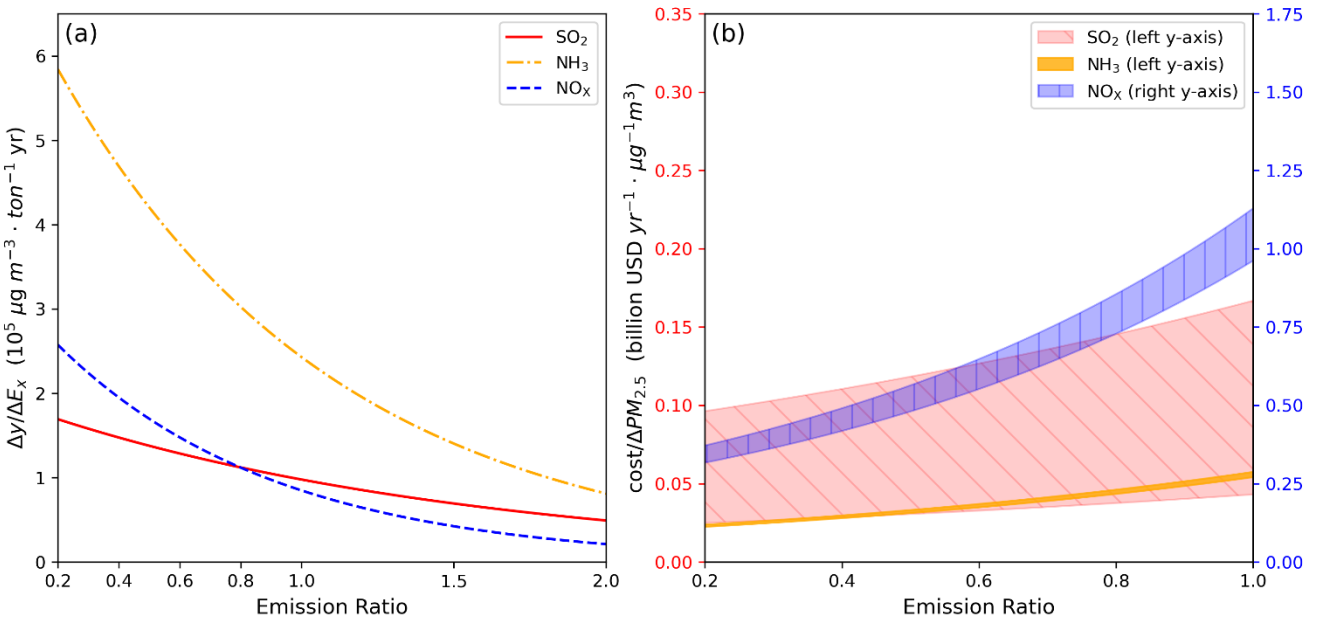

Figure 7: (a) $PM_{2.5}$ reduction efficiency and (b) reduction cost as a function of emission ratio for SO_2, NH_3, and NOx.